Optical design of cube-corner retroreflectors having curved mirror surfaces

Atsushi Minato, Nobuo Sugimoto, and Yasuhiro Sasano

The characteristics of retroreflectors that include curved mirror surfaces are theoretically investigated. The use of curved mirror surfaces in a cube-corner retroreflector is an effective method for diverging the reflected beam, especially in a large-aperture hollow retroreflector. The effect of curved surfaces is demonstrated for simple examples that give circular and elliptical wave-front patterns. The method was applied in the optical design of a satellite retroreflector in space, which is to be loaded on the Japanese polar orbit Advanced Earth Observing Satellite.

1. Introduction

A perfect cube-corner retroreflector reflects the incident beam into the exact reverse direction. This characteristic of a cube-corner retroreflector is used in various applications including laser remote sensing[1] and laser cavity design.[2] In some applications, however, a diverging reflected beam is required. One example would be to correct the velocity aberration in space applications. For these purposes, spoiled angles in a corner cube and a diverging lens in front of a corner cube have been utilized to control the direction and divergence of the reflected beam. However, the use of spoiled angles is practical only for a specific geometry of the light source and the retroreflector. The use of a lens is not practical for large-aperture retroreflectors and for applications in which the reflectors are used in wide spectral ranges.

We investigated the use of curved surfaces for mirrors that form a cube-corner retroreflector. We studied the effect of curved surfaces on the wave front and the far-field pattern of the reflected beam by a computer simulation. The result shows that the use of curved mirrors in a retroreflector is quite effective for controlling the divergence of the reflected beam.

We have applied the method to the design of a satelliteborne laser reflector named RIS (retroreflector in space), which is to be loaded on the Advanced Earth Observing Satellite (ADEOS) planned for launch in 1996. RIS is a hollow cube-corner retroreflector with a diameter of 0.5 m for earth–satellite–earth laser long-path absorption experiments.[3,4] The results of a computer simulation show that the combination of a spherical surface and **spoiled** angles works successfully for correcting the velocity aberration that changes with the satellite position relative to a ground station.

In this paper we first present a theoretical method to calculate the wave front of the reflected beam. In Section 3 we demonstrate the effect of curved surfaces for retroreflectors having a single spherical surface and three spherical surfaces. In Section 4 we describe the optical design of the RIS that uses a spherical surface and **spoiled** angles simultaneously.

2. Method for Wave-Front Calculation

First we consider a perfect retroreflector that is formed by three flat surfaces that are perpendicular to each other. The effect of curved surfaces is treated with an approximation, taking into consideration that the surface curvatures are small. Figure 1 shows the geometry considered in the calculation. Three flat mirrors are located in the x, y, and z planes. The position and direction of the reflections at each mirror surface can be traced for the ray incident on the retroreflector. There are six different orders of reflection at three mirrors.

We now consider the case in which a ray incident on the x plane is reflected by the y plane and then reflected by the z plane. If we indicate the direction cosine of the incident ray as (α, β, γ), the directions of the ray reflected by the x, y, and z planes are simply $(-\alpha, \beta, \gamma)$, $(-\alpha, -\beta, \gamma)$, and $(-\alpha, -\beta, -\gamma)$, respectively. The positions of the ray on the x, y, and z planes, $(0, y_1, z_1)$, $(x_2, 0, z_2)$, and $(x_3, y_3, 0)$, are obtained from a symmetrical consideration as illustrated in Fig. 1.

The authors are with The National Institute for Environmental Studies, 16-2 Onogawa, Tsukuba, Ibaraki 305, Japan.

Received 11 July 1991.
0003-6935/92/286015-06$05.00/0.
© 1992 Optical Society of America.

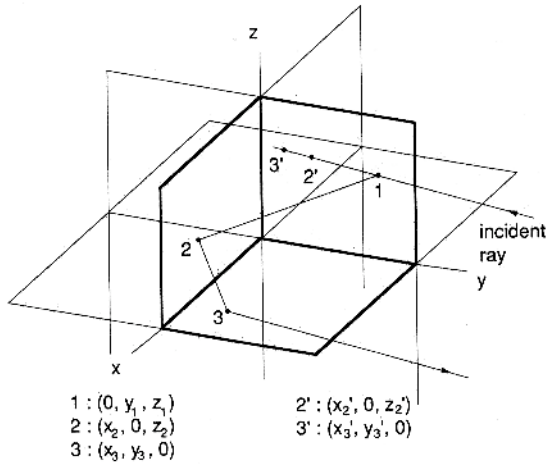

Fig. 1. Geometric model used for the theoretical calculations.

We assume that the ray incident on the x plane penetrates the x plane, y plane, and then the z plane. If we denote the positions of the ray on the x, y, and z planes as $(0, y_1, z_1)$, $(x_2', 0, z_2')$, and $(x_3', y_3', 0)$, then one also has the following relationships:

$$(x_2, 0, z_2) = (-x_2', 0, z_2'),$$
$$(x_3, y_3, 0) = (-x_3', -y_3', 0). \quad (1)$$

Since the positions $(0, y_1, z_1)$, $(x_2', 0, z_2')$, and $(x_3', y_3', 0)$ can be easily calculated when the direction and the position of the incident ray are given, we can calculate the position of the reflections on the actual retroreflector from Eqs. (1). We can calculate the positions of the reflections in the same manner for the other orders of reflection.

The effects of the slightly curved surfaces were included by considering the additional phase shift or optical path length at each reflection as illustrated in Fig. 2. We neglected the change in the position and direction of a ray inside the reflector that is due to the curvature bacause the resulting error in the position of the ray is negligibly small compared with the dimension of the retroreflector. The additional path length is calculated from the distance between the curved surface and the original flat surface at the position of the reflection. The additional path length

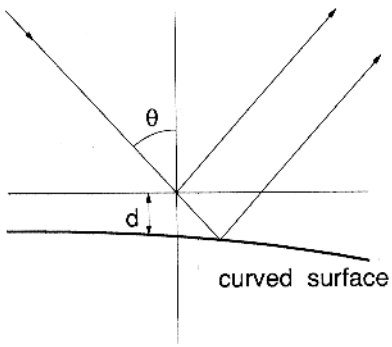

Fig. 2. Additional path length added to the reflection at a curved mirror surface.

can be written as

$$\Delta L = 2d \cos \theta, \quad (2)$$

where d represents the distance from the original flat surface and θ is the angle of incidence.

The additional path lengths at three reflections are summed to obtain the total phase shift. The phase shift can thus be written as

$$\Delta\varphi = (2\pi/\lambda)\Sigma_i(\Delta L)_i = (4\pi/\lambda)\Sigma_i d_i \cos \theta_i, \quad (3)$$

where λ is the wavelength of incident light, and i denotes x, y, and z. The wave front of the reflected beam is obtained by considering a grid in front of the retroreflector and calculating the phase shifts for the rays that pass through each point on the grid.

The deformation of the calculated wave front that is due to the approximation used in this calculation is of the order of $(d_{\max}/D)$, where $d_{\max}$ is the maximum distance in Eq. (2) and D is the dimension of the mirror panel. It was estimated to be $<0.01\%$ in the examples that are described in the following sections.

3. Retroreflector Having Spherical Surfaces

We present the results of the calculation for simple examples that give circular and elliptical wave-front patterns. Figure 3(a) shows the calculated interference fringes (wave front) at 632.8 nm for a retroreflector that includes a single spherical mirror. In Fig. 3 the direction cosine of the incident plane wave is assumed to be $-(1/\sqrt{3})$ (1, 1, 1), and the reflected beam is also observed from the $(1/\sqrt{3})$ (1, 1, 1) direction. The dimension of the mirror panels is 36 cm × 36 cm, and the z surface has a curvature with a radius of 17,000 m. The center of the sphere is located on the negative z axis. The reflector is a complete cube corner at the central portion. The z surface is expressed by the following equation:

$$x^2 + y^2 + (z + R)^2 = R^2, \quad (4)$$

where R is the radius of curvature. Because z is much smaller than R, d_z in Eq. (3) can be approximately written by

$$d_z(x, y) = -(1/2)\,(1/R)\,(x^2 + y^2). \quad (5)$$

The angle θ_z in Eq. (3) depends on the direction of the incident beam, and $\theta_z = 54.74°$ in this case. The phase shift was calculated for rays that pass through a 100 × 100 grid to obtain the wave front. The calculated wave front has an elliptical pattern as seen in Fig. 3(a). We can define focal lengths of the retroreflector for the major axis and minor axis directions separately. These can be written as

$$F_{\text{major}} = -(\sqrt{3}/2)R,$$
$$F_{\text{minor}} = -(1/2)\,(1/\sqrt{3})R. \quad (6)$$

Figures 3(b) and 3(c) show the interference fringes when the retroreflector is observed from different

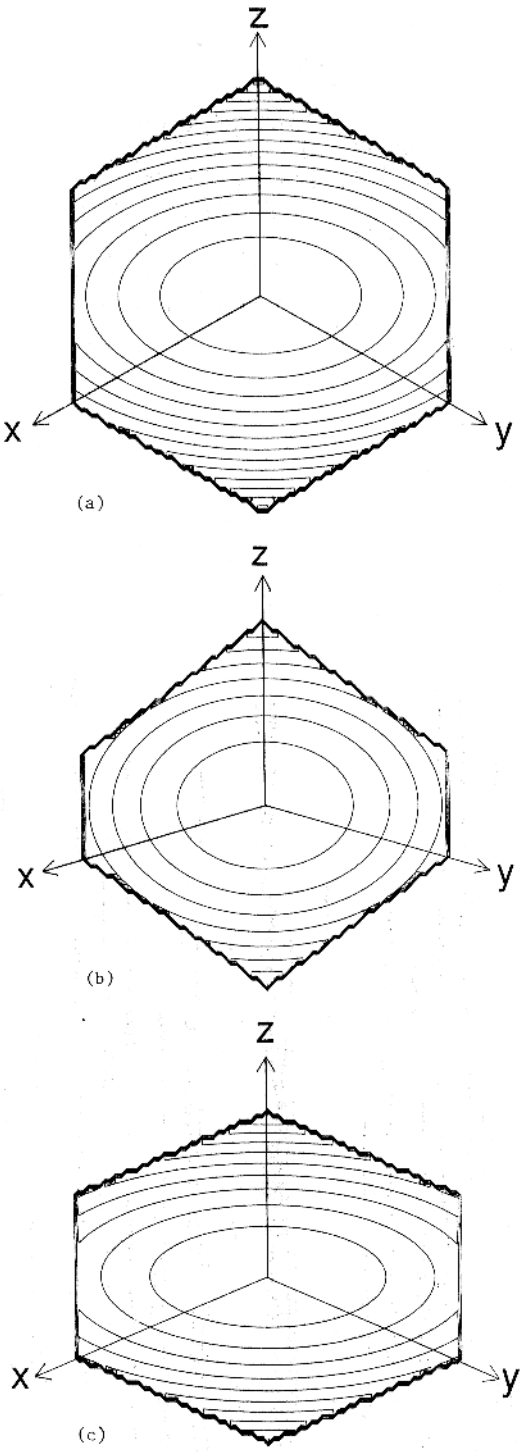

Fig. 3. Interference fringes of the reflected beams of a retroreflector having one spherical surface. Direction cosines of the incident beams are (a) $-(1/\sqrt{3})$ (1, 1, 1); (b) $-$(0.498, 0.498, 0.710); (c) $-$(0.639, 0.639, 0.427).

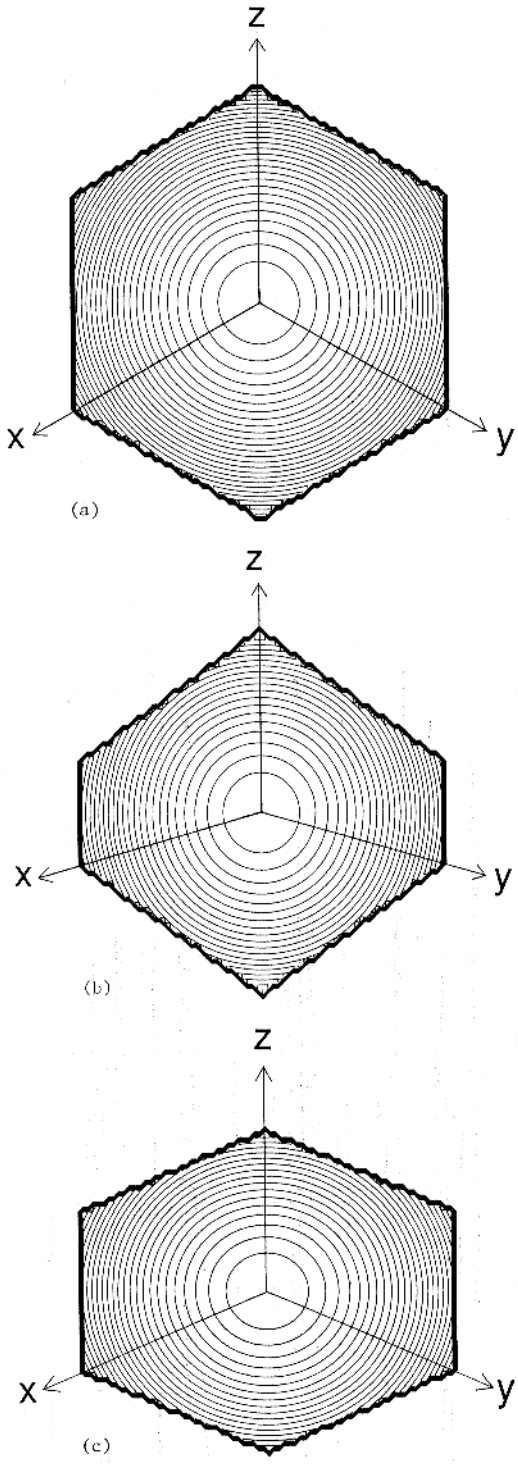

Fig. 4. Interference fringes of the reflected beams of a retroreflector having three spherical surfaces. Direction cosines of the incident beams are (a) $-(1/\sqrt{3})$ (1, 1, 1); (b) $-$(0.498, 0.498, 0.710); (c) $-$(0.639, 0.639, 0.427).

directions. The direction cosines of the incident beam are $-$(0.498, 0.498, 0.710) and $-$(0.639, 0.639, 0.427) for Figs. 3(b) and 3(c), respectively. The interference fringes also have elliptical structures. The shape of the ellipse changes with the direction of the incident beam as seen in Figs. 3(a)–3(c).

Figures 4(a)–(c) show the calculated interference fringes for a retroreflector with three spherical mirrors. The dimension of the reflector is the same as in Fig. 3. The surface curvature is the same for three mirrors and has a radius of 17,000 m. The centers of the spheres are located on the negative x, y, and z axes. The direction cosines of the incident

beam are $-(1/\sqrt{3})$ (1, 1, 1), $-(0.498, 0.498, 0.710)$, and $-(0.639, 0.639, 0.427)$ in Figs. 4(a), 4(b), and 4(c), respectively. The wave front has an axial symmetry when the incident beam direction is $-(1/\sqrt{3})$ (1, 1, 1). The focal length of the retroreflector is written as

$$F = -(1/4)\,(1/\sqrt{3})R. \tag{7}$$

The interference fringe becomes elliptical when observed from different directions. The direction of the major axis and the eccentricity of the ellipse depends on the beam direction. The eccentricity of the ellipse is ~ 0.01 for a 1° change in the beam direction from the $-(1/\sqrt{3})$ (1, 1, 1) direction.

A retroreflector with two spherical surfaces also has an elliptical wave-front pattern. We can also use concave spherical surfaces in retroreflectors that give converging beams with a similar wave-front pattern as seen in Figs. 3 and 4.

We can include spoiled angles simultaneously with curved surfaces. The effects of spoiled angles can be included directly into the surface shape function by adding linear terms. It is also possible to calculate the phase shift that is due to the spoiled angles separately and add the phase shift to the wave front of a curved retroreflector as long as the surface curvature and spoiled angles are small.

We can also calculate the wave front for a retroreflector that includes any surface shape by the method presented in Section 2. The interference fringe, in general, splits into six triangular regions and cannot be represented by a simple analytical shape.

4. Design of the Retroreflector in Space for the Advanced Earth Observing Satellite

RIS is a retroreflector for laser long-path absorption experiments to be loaded on the Japanese polar orbit satellite ADEOS. RIS is to be installed on the ADEOS so that the optical axis is directed to the ground with an angle of 30° toward the satellite movement from nadir. Because the altitude of the ADEOS orbit is $\sim$800km and the field of view of the RIS is $\sim$60° full angle, the RIS experiment is possible when the RIS passes over one of the ground tracks to within several hundred kilometers of a ground station. The experiment will be performed while the RIS is being captured by the ground station in the elevation angle range from 30° to 90°.

Because the RIS moves with a velocity of $\sim$7 km/s, the velocity aberration had to be considered in the design of the RIS. the angular change θ in the reflected beam is written as

$$\theta = (2v \sin \phi)/c, \tag{8}$$

where v is the speed of the satellite, ϕ is the elevation angle of the beam from a ground station, and c is the speed of light. The velocity aberration in the RIS experiments, consequently, is 25–50 μrad, depending on the position of the RIS relative to a ground station.

The optical structure that was designed for the RIS is illustrated in Fig. 5. A spherical surface is used for the z surface along with spoiled angles to cover the change of the velocity aberration. The z surface is expressed by

$$z(x, y) = -3.6 \times 10^{-5}\,(x^2 + y^2) - 6.5 \times 10^{-6}\,(x + y). \tag{9}$$

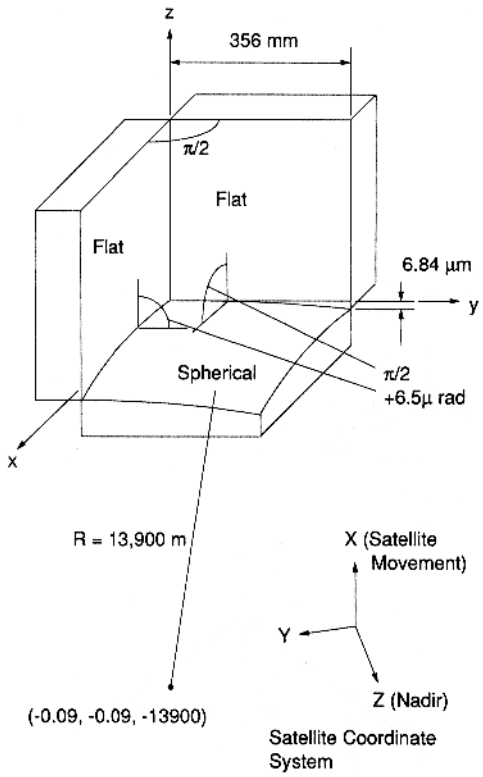

Fig. 5. Structure of the retroreflector for the RIS. Direction cosines of the x, y, z, and the optical axes of the RIS in the satellite coordinate system (X, Y, Z) are $(-0.079, 0.423, 0.903)$, $(-0.037, -0.906, 0.421)$, $(0.996, 0, 0.087)$, and $(0.508, -0.279, 0.815)$, respectively.

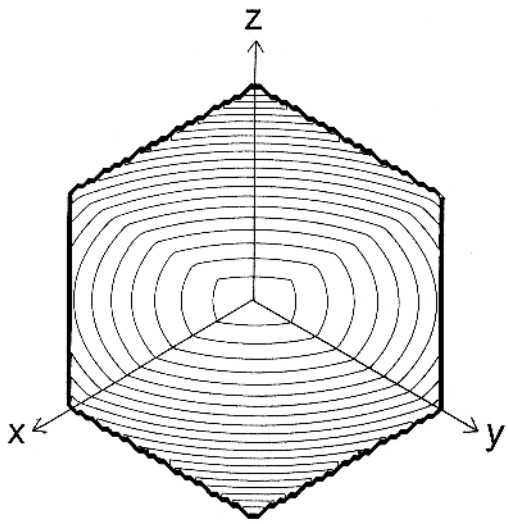

Fig. 6. Interference fringe of the RIS as observed from the direction of the optical axis.

Figure 6 shows the wave front of the reflected beam of the RIS at 632.8 nm as calculated by the method described in Section 2. The reflector is observed from the direction of the optical axis [i.e., the direction cosine is $(1/\sqrt{3})$ (1, 1, 1)], and the incident light is assumed to be a plane wave.

The intensity pattern of the reflected beam at a ground station was calculated from the wave front of the reflected beam at the RIS by using Kirchhoff's equation for the propagation of electromagnetic waves. The amplitude of the electric field at a point on the ground is written as

$$E_g = (aE_0/\lambda)|\Sigma_{ij} \exp[i[(2\pi/\lambda)r_{ij} + \varphi_{ij}]]|. \quad (10)$$

The subscripts i and j denote the grid points in front of the RIS for which the phase of the reflected light, φ_{ij}, is given. r_{ij} represents the distance between a grid point and a point on the ground. The coefficient a in Eq. (10) represents the area of a grid element, and E_0 represents the electric field at the grid, which was assumed to be homogeneous over the RIS aperture area. The effect of the velocity aberration is included by shifting the calculated beam pattern on the ground. This is a good approximation because the speed of the RIS is much smaller than the speed of light. Figures 7(a) and 7(b) show the ground intensity patterns of the reflected beams at 532 nm and 10 μm, respectively.

The surface parameters indicated in Fig. 5 and Eq. (8) were determined by optimizing the calculated received power at a ground station. The optimization was made by calculating the received power as a function of the satellite position relative to the ground station for many different sets of surface parameters. Figure 8 shows the relative intensity of the received light, E_g^2/E_0^2, for the optimized RIS at a ground station as a function of the relative satellite position. The surface parameters were determined so that the sufficient intensity that is required from the RIS experiment is received at each position of the RIS in the region shown in Fig. 8.

Use of the convex surface with the positive spoiled angles shown in Fig. 5 is essential in the RIS design because the effective aperture area on the z surface is changed when the incident beam direction is changed. When the elevation angle of the beam from a ground station is small, only the area of the z surface close to the center of the RIS is effective as a retroreflector. The effective area increases by increasing the elevation angle, and the entire z surface is used when the elevation angle is 60° and larger. Because the velocity aberration is smaller when the elevation angle is small, it is reasonable that the additional angles between the z surface and the x and y surfaces are smaller at the central portion and are larger at the outer portion. We can use a concave surface with negative spoiled angles for the RIS. The reflected beam, however, converges once and then diverges.

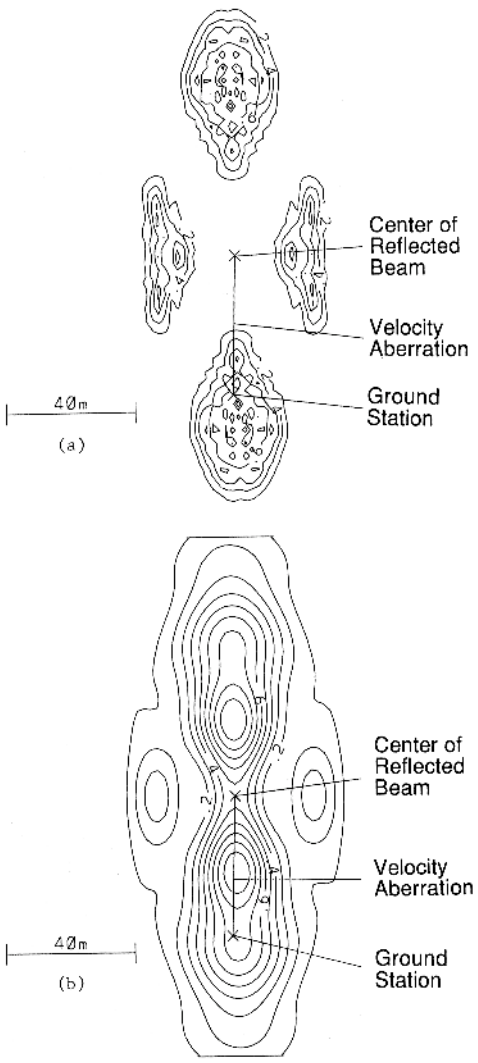

Fig. 7. Ground intensity pattern of the beam reflected by the RIS for the laser beam incident from the direction of the optical axis at (a) 532 nm; (b) 10 μm.

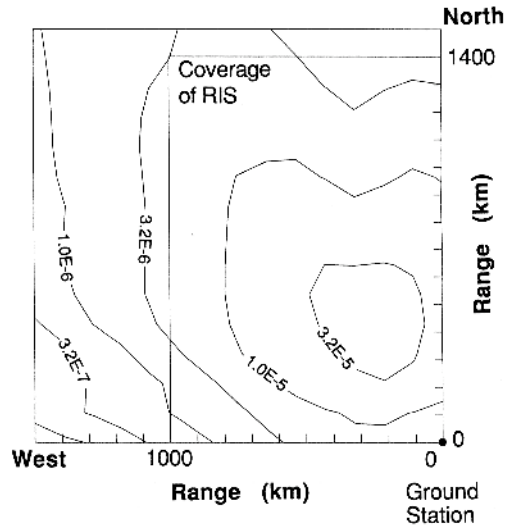

Fig. 8. Intensity of the reflected beam, E_g^2/E_0^2, as a function of the satellite position relative to a ground station. The region in which the RIS experiment is performed is shown for descending satellite paths.

5. Conclusion

We investigated the effects of curved mirror surfaces in a cube-corner retroreflector. It has been shown that the use of curved surfaces is a useful method to control the divergence of the reflected beam for a large-aperture hollow retroreflector for which a diverging lens is not usable. We have demonstrated the method for simple examples by giving circular and elliptical wave-front patterns. We also described the optical design of the RIS for which the use of a spherical surface along with spoiled angles is successfully applied for correcting the velocity aberration.

The method presented in this paper can also be applied to retroreflectors with concave surfaces. We obtained a converging spherical wave front, for example, by using three concave spherical surfaces. The characteristics of such retroreflectors are expected to be useful in applications such as laser cavity design.

References

1. R. M. Measures, *Laser Remote Sensing* (Wiley, New York, 1984).
2. G. Zhou, A. J. Alfrey, and L. W. Casperson, "Modes of a laser resonator with a retroreflecting corner cube mirror," Appl. Opt. **21,** 1670–1674 (1982).
3. N. Sugimoto, A. Minato, and Y. Sasano, "Retroreflector in-space (RIS) for Japanese satellite ADEOS," in *Abstract of Papers of the 15th International Laser Radar Conference* (Institute of Atmospheric Optics, Tomsk, 1990), Part I, p. 48.
4. N. Sugimoto, A. Minato, and Y. Sasano, "Retroreflector in-space for the ADEOS satellite," in *Conference on Lasers and Electro-Optics,* Vol. 10 of OSA 1991 Technical Digest Series (Optical Society of America, Washington, D.C., 1991), p. 450.